

# Electronic states in ferromagnetic $\text{Cr}_x\text{NbSe}_2$ ( $x = 0.33, 0.5$ ) studied by $^{53}\text{Cr}$ and $^{93}\text{Nb}$ NMR spectroscopy

V. V. Ogloblichev <sup>1,\*</sup>, N. V. Baranov <sup>1,2</sup>, P. A. Agzamova <sup>1</sup>, A. Yu. Germov <sup>1</sup>, N. M. Nosova,<sup>2</sup> Yu. V. Piskunov <sup>1</sup>,  
E. M. Sherokalova <sup>2</sup>, N. V. Selezneva,<sup>2</sup> A. F. Sadykov <sup>1</sup> and A. G. Smolnikov<sup>1</sup>

<sup>1</sup>*M. N. Mikheev Institute of Metal Physics, Ural Branch, Russian Academy of Sciences, Yekaterinburg 620108, Russian Federation*

<sup>2</sup>*Institute of Natural Science, Ural Federal University, Yekaterinburg 620083, Russian Federation*



(Received 28 July 2021; revised 15 October 2021; accepted 24 November 2021; published 9 December 2021)

The results of investigation of the  $\text{Cr}_x\text{NbSe}_2$  chalcogenides ( $x = 0.33, 0.5$ ) by the nuclear magnetic resonance (NMR) method on  $^{53}\text{Cr}$  and  $^{93}\text{Nb}$  nuclei in the magnetically ordered state at zero external magnetic field have been presented. *Ab initio* calculations have been performed to theoretically estimate NMR parameters and interpret the experimental data. It has been shown that the intercalation of Cr atoms into  $\text{NbSe}_2$  results in spin and charge redistributions. The lower magnetic moment of chromium nuclei,  $2.2 \mu_B$ , compared to the theoretical value  $\mu = 3 \mu_B$  for  $\text{Cr}^{3+}$  is attributed to the high degree of hybridization of the  $a_{1g}$  and  $e_g$  orbitals of  $3d$  Cr electrons with  $4d_{z^2}$  and  $5s$  niobium orbitals. Such a hybridization also results in the presence of a high local magnetic field in the niobium nuclei location in  $\text{Cr}_x\text{NbSe}_2$ .

DOI: [10.1103/PhysRevB.104.245115](https://doi.org/10.1103/PhysRevB.104.245115)

## I. INTRODUCTION

The transition metal dichalcogenides (TMDCs) and their intercalates have been the subject of increasingly active study in the fields of physics, chemistry, materials science, and nanotechnology due to their intriguing physical and chemical properties and potential applications. Depending on the type of transition metal ( $M$ ) and chalcogen ( $X$ ) atoms the  $\text{MX}_2$  compounds can be metallic, semiconducting, or insulating; in the bulk form, the  $\text{MX}_2$  compounds demonstrate paramagnetic or diamagnetic behavior [1,2]. Intensive studies of TMDCs performed in recent decades have shown that the electronic structure and properties of these compounds can be significantly different in bulk and monolayer state or with additional atoms introduced between the  $X$ - $M$ - $X$  trilayers. The  $2H$ - $\text{NbX}_2$  compounds ( $X = \text{S}, \text{Se}$ ) are typical examples of this type of material. They exhibit metallic type conductivity behavior and transition to the superconducting state with decreasing temperature below 5.7 and 7.2 K in sulfide and selenide compounds, respectively (see Ref. [3], for instance). It was revealed that the intercalation of  $3d$  metal atoms ( $M'$ ) into  $2H$ - $\text{NbS}_2$  and  $2H$ - $\text{NbSe}_2$  not only suppresses superconductivity, but also generates various magnetic states in  $M'_x\text{NbX}_2$  depending on the type and concentration of intercalated  $M'$  atoms as well as on the type of the parent compound [4–6].

Thus the  $\text{Cr}_{0.33}\text{NbS}_2$  compound intercalated with chromium was observed to exhibit the long-period helimagnetic structure [7,8] which can be transformed into a chiral soliton lattice under the application of a magnetic field [8–10]. The chiral soliton lattice in bulk and in exfoliated  $\text{Cr}_{0.33}\text{NbS}_2$  crystals was observed to exhibit unusual properties [11,12]. Meanwhile, the selenide compounds

$\text{Cr}_x\text{NbSe}_2$  with  $x \geq 0.33$  demonstrate ferromagnetic ordering [6,13]. The comparative study of the electronic structure of the parent compound  $\text{NbS}_2$  and  $\text{Cr}_{0.33}\text{NbS}_2$  by using photoelectron spectroscopy methods [14] has shown that the insertion of Cr atoms between S-Nb-S sandwiches leads to the changes in local electronic environment of Nb atoms and results in the transfer of electron charge from chromium to the  $\text{NbS}_2$  layers, although the Cr intercalation does not substantially alter the two-dimensional character of  $\text{NbS}_2$  electronic structure [15]. The Cr- and Nb-derived electronic states are found to be strongly hybridized in  $\text{Cr}_{0.33}\text{NbS}_2$  [14,15]. These findings together with the density functional theory calculations imply a substantial role of the Hund's exchange interaction between the itinerant electrons and local spin moments in the formation of magnetic order in the compound [15]. In contrast to sulfide compound  $\text{Cr}_{0.33}\text{NbS}_2$ , the literature data on the features of the electronic structure and charge and spin density distribution in the selenide  $\text{Cr}_x\text{NbSe}_2$  compounds intercalated with Cr atoms are insufficient. The band structure calculations and optical spectroscopy studies performed for the ferromagnetic  $\text{Cr}_{0.33}\text{NbSe}_2$  compound have revealed strong hybridization of the Cr  $3d$  and Nb  $4d$  states as well. Moreover, the conducting band broadening was observed with the decreasing temperature below the Curie temperature [16]. According to the recent studies of crystal structure, magnetic, transport, and thermal properties of the  $\text{Cr}_x\text{NbSe}_2$  family ( $0 < x \leq 0.5$ ) all the compounds exhibit the metallic type resistivity behavior and the cluster-glass magnetic state at  $x < 0.33$ , while a soft ferromagnetic behavior was observed in compounds with higher Cr contents ( $x \geq 0.33$ ) [6]. Using the  $^{53}\text{Cr}$  nuclear magnetic resonance (NMR) spectroscopy the valence state of Cr atoms in compounds  $\text{Cr}_x\text{NbSe}_2$  with  $x = 0.33$  and  $x = 0.5$  was determined to be close to  $\text{Cr}^{4+}$  [6], as the Cr valence state revealed recently in the  $1T$ - $\text{CrSe}_2$

\*ogloblichev@imp.uran.ru

compound [17]. The reduction of the average magnetic moment per Cr atom in saturation observed in  $\text{Cr}_x\text{NbSe}_2$  was ascribed to the possible appearance of magnetic moment on Nb atoms oppositely directed relative to the Cr moment.

Bearing in mind that the distribution of charge and spin density is a key to understanding the mechanisms responsible for the changes in structural, magnetic, and transport properties of compounds upon intercalation of various TMDCs the present work aims to study the  $\text{Cr}_x\text{NbSe}_2$  compounds with chromium concentration  $x = 0.33$  and  $x = 0.5$  by means of NMR spectroscopy on  $^{53}\text{Cr}$  and  $^{93}\text{Nb}$  nuclei. Attention will mainly be paid to reveal how the intercalation of Cr atoms into  $\text{NbSe}_2$  affects the electron configuration and magnetic state of Nb atoms. Along with the measurements of the NMR spectra, *ab initio* calculations were performed to estimate the quadrupole interactions of chromium and niobium nuclei in different environments.

## II. SAMPLES AND METHODS

Polycrystalline  $\text{Cr}_{0.33}\text{NbSe}_2$  and  $\text{Cr}_{0.5}\text{NbSe}_2$  samples studied in the present work were synthesized by the two-stage solid-state reaction method, which was used in our previous work [6] to obtain the  $\text{Cr}_x\text{NbSe}_2$  compounds with various chromium within the range  $0 \leq x \leq 0.5$ . The obtained specimens were milled, compacted into pellets, and then homogenized for 120 h at 800 °C. X-ray diffraction analysis performed by using a Bruker D8 Advance diffractometer and FULLPROF software has shown that the samples with Cr concentrations  $x < 0.5$  are single phase, while the compound  $\text{Cr}_{0.5}\text{NbSe}_2$  contains a small amount (~5%) of foreign phases. As follows from the measurements of the temperature dependences of the magnetic susceptibility and field dependences of the magnetization, the  $\text{Cr}_{0.33}\text{NbSe}_2$  and  $\text{Cr}_{0.5}\text{NbSe}_2$  compounds enter a long-range ferromagnetic order with decreasing temperature below  $T_C \approx 82$  K and  $T_C \approx 65$  K, respectively [6].

The NMR measurements were performed on the advanced pulse spectrometer SXP 4100 (Bruker) at  $T = 4.2$  K (samples were in direct contact with liquid helium) in zero external magnetic field. Frequency band  $\nu = 40\text{--}320$  MHz was scanned at the signal search. The NMR spectra were obtained by standard spin-echo technique  $p\text{--}t_{\text{del}}\text{--}2p\text{--}t_{\text{del}}\text{--}E(2t_{\text{del}})$  at the frequency change of sample irradiation. The duration of the first pulse was  $p = 1$   $\mu\text{s}$ ; the power of the rf amplifier 50–100 W. For spectra recording the summation of Fourier signals stored in the whole frequency band with a step  $\Delta\nu = 300$  kHz was applied. The measurements of  $^{53}\text{Cr}$  and  $^{93}\text{Nb}$  NMR spectra were carried out at the delay between pulses  $t_{\text{del}} = 20$   $\mu\text{s}$  and  $t_{\text{del}} = 9$   $\mu\text{s}$ , correspondingly. The time of spin-spin relaxation was measured at the maximum NMR signal from  $^{93}\text{Nb}$  nuclei at frequency  $\nu \approx 166$  MHz under the change of delay time between pulses  $t_{\text{del}}$  in the pulse sequence of spin echo.

The experiment repetition time was 200 ms which is greater than  $20 \times T_1$ , where  $T_1$  is the spin-lattice relaxation time ( $T_1 < 2$  ms). Such a long repetition time was chosen to avoid the influence of local heating of the samples due to the metallic nature of their conductivity [6]. In order to calculate the shape of NMR lines the spectra modeling program SIMUL [18–21] was used. It numerically calculates the line shape

based on the complete Hamiltonian of the nuclear system taking into account Zeeman and quadrupole contributions and spatial orientation of magnetic moments of chromium atoms.

To evaluate the parameters of the NMR spectra, *ab initio* calculations were carried out using the projected augmented wave method (PAW) [22] and PBE (Perdew-Burke-Ernzerhof) exchange-correlation functional [23] realized in the computational package VASP (Vienna *ab initio* simulated package) [24]. The exchange-correlation interaction was taken into consideration in the general gradient approximation (GGA) with regard to spin-orbit coupling (SOC). The net with a set of  $k$  points  $4 \times 4 \times 4$  was used for calculations.

## III. RESULTS AND DISCUSSION

### A. $^{53}\text{Cr}$ NMR data

The first results of the investigation of polycrystalline samples  $\text{Cr}_{0.33}\text{NbSe}_2$  and  $\text{Cr}_{0.5}\text{NbSe}_2$  by the NMR method on the  $^{53}\text{Cr}$  nuclei (spin  $^{53}I = 3/2$ , gyromagnetic relationship  $^{53}\gamma/2\pi = 0.240$  64 MHz/kOe) were presented in our previous work [6]. This work provides a detailed analysis of the NMR spectra together with *ab initio* calculations of the NMR parameters.

The typical NMR spectrum of  $^{53}\text{Cr}$  nuclei has a central line corresponding to the  $m_{-1/2 \leftrightarrow 1/2}$  transition and two satellite lines corresponding to the  $m_{\pm 3/2 \leftrightarrow \pm 1/2}$  transitions. This structure results from the interaction of nuclear quadrupole moment  $Q$  with the electric-field gradient (EFG) produced in the nuclei location by their charge environment [19,25]. The position of the resonance frequencies of the central line and satellites is determined by the EFG tensor components  $V_{ij}$  ( $i, j = x, y, z$ ):

$$\nu_Q = \frac{3eV_{zz}Q}{2I(2I-1)h} = \frac{3}{2I(2I-1)}Q_{CC}; \quad \eta = \frac{V_{yy} - V_{xx}}{V_{zz}}, \quad (1)$$

where  $\nu_Q$  is the quadrupole frequency;  $Q_{CC}$  is the nuclear quadrupole interaction constant;  $h$  is the Planck constant;  $\eta$  is the EFG asymmetry parameter. It should be mentioned that in the nuclear magnetic resonance community, the zero-field NMR spectrum is usually referred to as nuclear quadrupole resonance (NQR). An NQR study [26] of the initial superconducting compound  $2\text{H-NbSe}_2$  on the  $^{93}\text{Nb}$  nuclei revealed an NQR spectrum corresponding to the  $7/2 \leftrightarrow 9/2$  transition near the frequency  $\nu_{\text{res}} \approx 10$  MHz, which corresponds to the quadrupole frequency  $\nu_Q \approx 2.53$  MHz. However, in our case, the resonance frequencies of the  $^{53}\text{Cr}$  and  $^{93}\text{Nb}$  nuclei,  $\nu_{\text{res}}$ , are much higher than their quadrupole frequencies,  $\nu_Q$ . The resonance spectra observed in  $\text{Cr}_x\text{NbSe}_2$  are mainly determined by the interaction of nuclear spin moments with internal local magnetic fields. Therefore, we observe NMR spectra in a local magnetic field, not NQR.

The chromium NMR spectrum (Fig. 1) in the sample with  $x = 0.5$  is well fitted by one line, 1. Unlike  $x = 0.5$  the  $^{53}\text{Cr}$  NMR spectrum of  $\text{Cr}_x\text{NbSe}_2$  with  $x = 0.33$  can be described by only the superposition of two quadrupole split lines, 2, 3. The existence of two lines in the NMR spectrum of  $^{53}\text{Cr}$  nuclei indicates the presence of two chromium ion positions with a different nearest magnetic and/or charge environment in the structure.

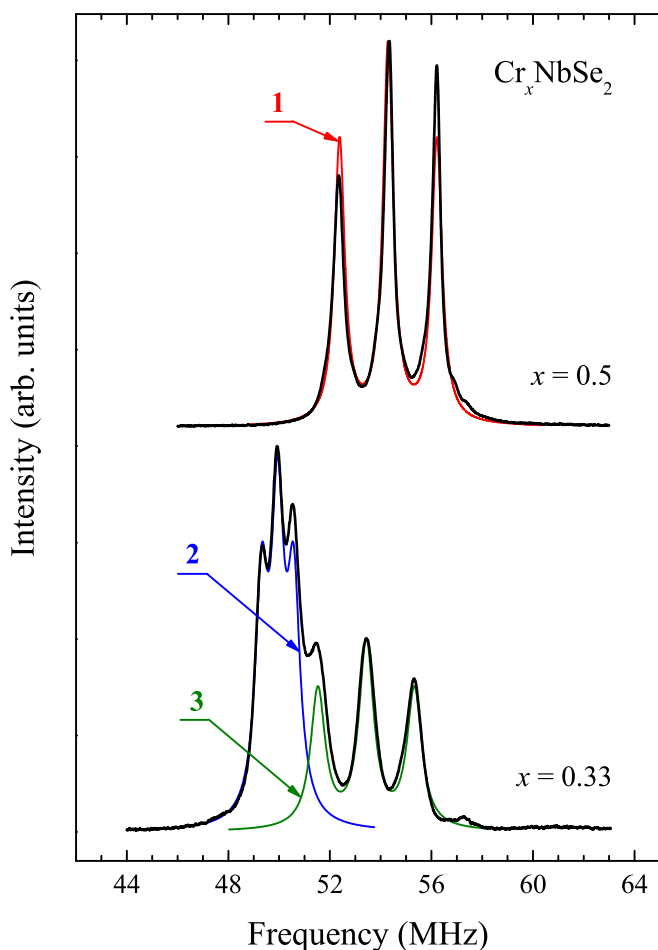


FIG. 1.  $^{53}\text{Cr}$  NMR spectrum in  $\text{Cr}_x\text{NbSe}_2$  ( $x = 0.33, 0.5$ ) at temperature  $T = 4.2\text{ K}$  in zero external magnetic field. Solid lines show the result of modeling the experimental spectrum with three quadrupole split lines.

Intercalation of the parent compound  $\text{NbSe}_2$  with chromium ions leads to the formation of crystal structures

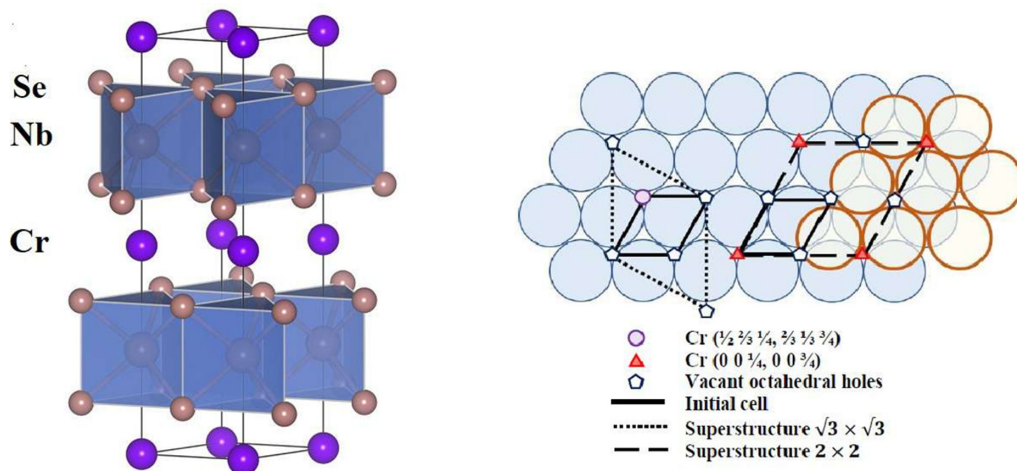


FIG. 2. Side view (left) and planar view (right) of the crystal structure of  $\text{Cr}_x\text{NbSe}_2$  (the solid line denotes the initial cell, the dashed line  $2 \times 2$  ordering, and the dotted line  $\sqrt{3} \times \sqrt{3}$  ordering of Cr atoms).

with a different arrangement of chromium atoms in the lattice [6,9]. Figure 2 shows a scheme of the crystal structure of  $\text{Cr}_x\text{NbSe}_2$  with a trigonal-prismatic surrounding of Nb and octahedral positions between Se-Nb-Se sandwiches which can be occupied by intercalated Cr atoms; possible orderings of Cr atoms between prismatic layers are displayed as well (see right panel).

In the sulfide compounds  $\text{Cr}_x\text{NbS}_2$ , the Cr ions can also occupy different crystallographic positions (see Ref. [27], for instance). According to the x-ray diffraction (XRD) data [6] the  $\text{Cr}_x\text{NbSe}_2$  samples with Se concentrations  $x < 0.25$  are isostructural to the  $2H\text{-NbSe}_2$  matrix and have a crystal lattice belonging to the space group  $P6_3/mmc$ , while ordering of Cr atoms leads to the formation of the  $2 \times 2$  superstructure in  $\text{Cr}_{0.25}\text{NbSe}_2$ . For the compositions  $0.25 < x < 0.50$ , chromium atoms become ordered in the  $ab$  plane with the formation of the  $\sqrt{3} \times \sqrt{3}$  superstructure (space group  $P6_322$ ) with respect to the structure of  $\text{NbSe}_2$ . From the absence of clear visible superstructure reflections on the powder XRD pattern, the crystal structure of the  $\text{Cr}_{0.5}\text{NbSe}_2$  compound was attributed the  $P6_3/mmc$  space group [6]. However, it is important to note here that in the related  $2H\text{-Fe}_x\text{NbSe}_2$  and  $2H\text{-Fe}_x\text{TaSe}_2$  systems, using scanning tunneling microscopy revealed the coexistence in crystals of regions with different ordering [28]. In particular, at  $x = 0.33$ , the coexistence of regions with orderings of the  $2 \times 2$  ( $P6_3/mmc$ ) and  $\sqrt{3} \times \sqrt{3}$  ( $P6_322$ ) type was observed in these compounds [28]. Therefore, it can be assumed that such coexistence also takes place in  $\text{Cr}_{0.33}\text{NbSe}_2$ . The NMR method does not allow us to directly associate the observed NMR spectrum with a particular space group. However, the NMR spectroscopy identifies differences in local symmetry at the positions of resonating nuclei probes. Thus the proximity of the NMR parameters (see Table I) of line 2 for  $x = 0.33$  and line 3 for  $x = 0.5$  indicates that Cr atoms can be located in positions with an identical environment despite the different concentrations of the intercalant.

For the crystal structures  $P6_3/mmc$  and  $P6_322$  the parameters of quadrupole interaction of chromium nuclei were determined by the first-principles calculations using density

TABLE I. Parameters of the lines used to simulate the experimental  $^{53}\text{Cr}$  [6] and  $^{93}\text{Nb}$  NMR spectra presented in Figs. 1 and 4.

Line	$\text{Cr}_{0.50}\text{NbSe}_2$				$\text{Cr}_{0.33}\text{NbSe}_2$					
	$^{53}\text{Cr}$		$^{93}\text{Nb}$		$^{53}\text{Cr}$		$^{93}\text{Nb}$			
	1				2	3				
	Expt.	Calc.	Expt.	Calc.	Expt.	Calc.	Expt.	Calc.	Expt.	Calc.
$\nu_Q$ (MHz)	3.82(6)	2.85	0.264(10)	1.2	1.24(6)	1.11	3.82(6)	2.85	0.250(10)	0.8-1.2
$\eta$	—	0	—	0	—	0	—	0	—	0
$h_{\text{loc}}$ (kOe)	225.7	—	158.1	—	207.7	—	222.1	—	160	—

functional theory (DFT) methods in the VASP program package (the lattice parameters for  $x = 0.33$  and  $x = 0.5$  were taken from Ref. [6]). It was determined that for both structures the principal axis of the electric-field gradient  $V_{zz}$  is directed along the  $c$  axis and has the asymmetry parameter  $\eta$  close to zero. The values of quadrupole frequencies are determined as  $\nu_Q^{\text{calc}} = 1.1$  MHz for the crystal structures with the  $P6_3/mmc$  space group and  $\nu_Q^{\text{calc}} = 2.85$  MHz with the  $P6_322$  space group, respectively (see Table I).

The NMR spectra on  $^{53}\text{Cr}$  nuclei were obtained in the local field, which in our case plays the role of an external magnetic field. Taking into account that the magnetic moments of chromium ions lie in the  $ab$  plane, the local field should also lie in this plane. Therefore, the angle between the main axis of EFG and the local field should be  $90^\circ$ . Consequently, the observed value of quadrupole frequency will be equal to the distance between satellite lines [19,25]. Based on the results obtained, line 2 in the  $\text{Cr}_{0.33}\text{NbSe}_2$  sample can be associated with chromium ions in the local environment as in the crystal structure of  $\text{Cr}_{0.25}\text{NbSe}_2$  due to the possible coexistence of regions with two superstructures (see above). Electron microscopic studies of single-crystalline samples are needed to support this assumption. As for line 1 in  $\text{Cr}_{0.5}\text{NbSe}_2$  and line 3 in  $\text{Cr}_{0.33}\text{NbSe}_2$ , they can be related to chromium ions located in local regions characteristic of the crystal structure described by the space group  $P6_322$ . It should be noted that the only one  $^{53}\text{Cr}$  NMR line (line 1) is observed in  $\text{Cr}_{0.5}\text{NbSe}_2$ . Therefore, based on the analysis of NMR data and first-principles calculations, the structure of  $\text{Cr}_{0.5}\text{NbSe}_2$  can most likely be assigned to the space group  $P6_322$ ; hence additional studies of the structure of this compound on a single-phase sample would be useful. The ratio of the integrated intensities of the two NMR lines for  $\text{Cr}_{0.33}\text{NbSe}_2$  gives the value  $\text{Int}(2)/\text{Int}(3) = 1.37$ , which characterizes the ratio of regions with superstructures described by space groups  $P6_3/mmc$  and  $P6_322$ .

Let us consider now the  $^{53}\text{Cr}$  NMR line shift. In the magnetically ordered state the  $^{53}\nu_{\text{res}}$  NMR frequency of chromium nuclei is determined by the local magnetic field  $h_{\text{loc}}$  ( $^{53}\nu_{\text{res}} = ^{53}\gamma h_{\text{loc}}$ ) in  $^{53}\text{Cr}$  nuclei location. The field  $\mathbf{h}_{\text{loc}}$ , in the simple case, includes the dipole field  $\mathbf{h}_{\text{loc,dip}}$ , and hyperfine field  $\mathbf{h}_{\text{loc,hf}}$  (HFF) [25,29]:

$$\mathbf{h}_{\text{loc}} = \mathbf{h}_{\text{loc,hf}} + \mathbf{h}_{\text{loc,dip}}. \quad (2)$$

Analyzing the local field in our previous work [6] we made the supposition that the value of dipole field  $\mathbf{h}_{\text{loc,dip}}$  can be

neglected because of its smallness. To support this supposition, in the present work, we carried out the calculations of  $\mathbf{h}_{\text{loc,dip}}$  field produced by the neighboring chromium magnetic moments in the case of ferromagnetic ordering in the  $ab$  plane. The calculation was performed within 50 coordination spheres with the use of common expression [29–31]. The calculation results have shown that the dipole fields  $\mathbf{h}_{\text{loc,dip}}$  produced on chromium ion lie along the direction of the chromium magnetic moments. The obtained  $\mathbf{h}_{\text{loc,dip}}$  values are equal to 36 and 45 Oe/ $\mu_B$  for crystal structures belonging to the  $P6_3/mmc$  and  $P6_322$  space groups, respectively. According to the theoretically possible value of the chromium magnetic moment,  $\mu = 3 \mu_B$ , the dipole field does not exceed 0.15 kOe which is three orders less than the observed field values  $\mathbf{h}_{\text{loc}}$  (see Table I) and therefore it can indeed be neglected.

Hyperfine field  $\mathbf{h}_{\text{loc,hf}}$  includes two contributions:

$$\mathbf{h}_{\text{loc,hf}} = g\mu_B(\mathbf{A}\mathbf{S}_i + \sum_j B_j \mathbf{S}_j), \quad (3)$$

where  $g$  is the  $g$  factor;  $\mathbf{S}_i$  is the electronic spin on site;  $\mathbf{S}_j$  is the electronic spin on the  $j$ th site. The first and second terms are, respectively, the on-site and supertransferred hyperfine interactions. The first term in the equation results from the magnetism of unpaired  $3d$  electrons of the chromium ion, and the second term corresponds to the spin polarization transfer from the nearest magnetic environment of the chromium ion [29]. Let us consider each of them.

The influence of spin-orbit coupling (SOC) in  $\text{Cr}_x\text{NbSe}_2$  compounds on the magnetization and other NMR parameters is rather small according to our first-principles calculations (less than 1%), which is in agreement with the data on isostructural  $\text{Cr}_{0.33}\text{NbS}_2$  [32]. Taking this into account, the main contribution to the local field at the Cr nucleus will be made by the spin magnetic moments of intrinsic  $3d$  electrons. The constant of hyperfine interaction between nuclear magnetic moments and  $3d$  electron is  $A \approx -100 \text{ kOe}/\mu_B$  [29,33,34].

The second contribution in Eq. (3) is connected with the spin polarization transfer from the nearest chromium magnetic ions. In the case of small chromium concentration and space group  $P6_3/mmc$ , the possibility of closely located chromium atoms should be low. That is why the second contribution in Eq. (3) can be considered as close to zero.

With an increase in the number of intercalated chromium atoms, the chromium-chromium interaction appears [35–39]. It should be noted that the spin polarization transfer from ions of the nearest magnetic environment has a short-range character [29]. The difference in local fields  $\Delta h_{\text{loc}} = 14.4 \text{ kOe}$

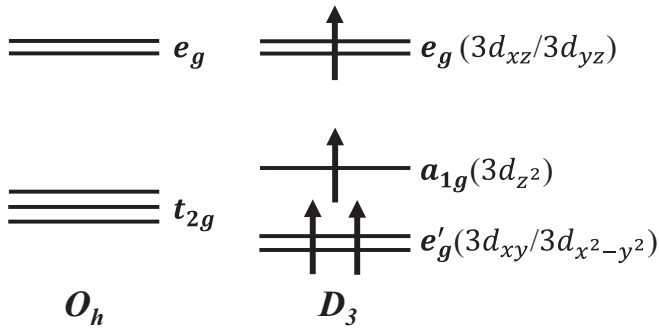


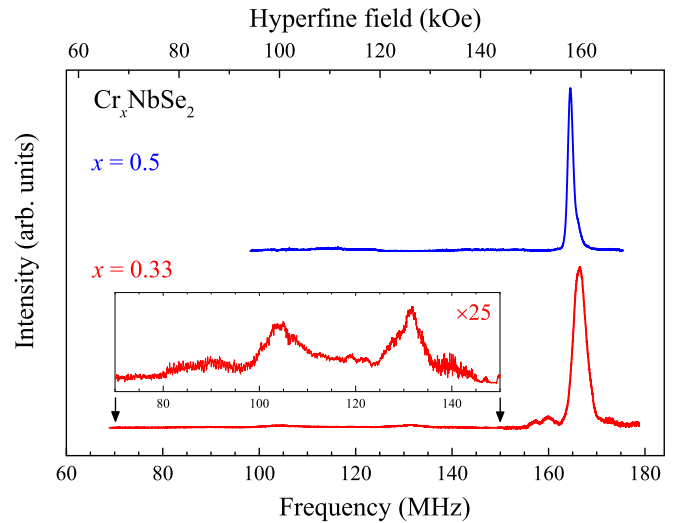
FIG. 3. Crystalline field splitting of Cr 3d level [27].

between lines 2 and 3 for  $\text{Cr}_{0.33}\text{NbSe}_2$  can be connected with the constant  $B_j$ . There should be more Cr-Cr bonds for the composition  $\text{Cr}_{0.5}\text{NbSe}_2$  unlike with the composition  $\text{Cr}_{0.33}\text{NbSe}_2$ . This was confirmed by our  $^{53}\text{Cr}$  NMR data: Line 2 is absent, and lines 1 and 3 have close values of quadrupole frequency  $\nu_Q$  and local field  $\mathbf{h}_{\text{loc}}$ .

In order to estimate the magnetic moment of chromium atoms the values  $h_{\text{loc}}$  obtained from the spectra in Fig. 1 were used. Thus we obtained the value  $\mu_{\text{NMR}} \approx 2.2 \mu_B$  from formula ([3]) for  $\text{Cr}_{0.33}\text{NbS}_2$  and  $\text{Cr}_{0.5}\text{NbS}_2$  compounds. The obtained value is less than the theoretical value of  $3 \mu_B$  for the high-spin state of the  $\text{Cr}^{3+}$  ion. It is closer to the  $\text{Cr}^{4+}$  valence state [40,41] and, on the whole, is in agreement with the data obtained at the study of the magnetization [6].

The decrease in the chromium magnetic moment in these compounds can be associated with the following. Each Cr ion has six selenium ions in the nearest neighborhood at the distance 2.43 Å and two niobium ions at the distance 3.00 Å [6]. In such a  $\text{CrSe}_6\text{-Nb}_2$  cluster, the local Cr environment does not have an orthorhombic  $O_h$  symmetry anymore, but it has the symmetry of trigonal prism  $D_3$ . In this case, the crystal field splits the fivefold degenerate Cr 3d states into one singly degenerate  $a_{1g}$  state with symmetry  $z^2$  and two doubly degenerate  $e'_g$  and  $e_g$  states with symmetry  $x^2 - y^2$ ,  $xy$ , and  $xz$ ,  $yz$ , respectively [42] (see Fig. 3).

Recently, the electronic structure of the  $\text{CrNb}_3\text{S}_6$  sulfide close to  $\text{Cr}_x\text{NbSe}_2$  was investigated and described in [32]. The authors found the following occupancy of Cr 3d orbitals:  $n(e'_g) = 1.8$ ,  $n(a_{1g}) = 0.76$ , and  $n(e_g) = 0.45$  with full spin  $S = \frac{3.01}{2}$ , as observed in the experiment. Also, the electronic states  $1.8 \ 3d_{xy}/3d_{x^2-y^2}$  in the  $e'_g$  orbital are well below the Fermi level. These electrons are well localized and do not take part in the covalent bond with ions of niobium and selenium. As for the electrons of  $3d_{zx}/3d_{zy}$  and  $3d_{z^2}$  orbitals, whose states cross the Fermi level, they are delocalized and have a high degree of hybridization with Nb  $4d_{z^2}$  orbitals and Se  $4p$  orbitals [32]. Our results show that only a portion of the electrons in the  $a_{1g}$  and  $e_g$  chromium orbitals,  $n = 0.35$  in  $\text{Cr}_{0.33}\text{NbSe}_2$  and  $n = 0.5$  in  $\text{Cr}_{0.5}\text{NbSe}_2$ , make a contribution to the creation of a local magnetic field on Cr nuclei. The rest are involved in the creation of induced hyperfine fields on the nuclei of niobium and selenium ions, which will be discussed below.

FIG. 4.  $^{93}\text{Nb}$  NMR spectrum in  $\text{Cr}_x\text{NbSe}_2$  ( $x = 0.33, 0.5$ ) at temperature  $T = 4.2$  K in zero external magnetic field. Inset shows an enlarged part of the spectrum for  $x = 0.33$  in the range 70–150 MHz.

### B. $^{93}\text{Nb}$ NMR data

In order to detect the hybridization of the 3d chromium states with the 4d niobium states, the NMR spectra measurements were performed on the  $^{93}\text{Nb}$  nucleus in polycrystalline samples  $\text{Cr}_x\text{NbSe}_2$  ( $x = 0.33, 0.5$ ) in zero external magnetic field at temperature  $T = 4.2$  K; these data are shown in Fig. 4. Isotope  $^{93}\text{Nb}$  has a spin  $^{93}I = 9/2$ , a natural abundance of 100%, a gyromagnetic ratio  $^{93}\gamma/2\pi = 10.421$  MHz/T, and a quadrupole nuclear moment  $Q = -0.28$  barn [43]. The position of the  $^{93}\text{Nb}$  NMR line, as in the case of  $^{53}\text{Cr}$  NMR, is determined by the local field  $\mathbf{h}_{\text{loc}}$  (formula 2). Figure 4 shows that the local-field values of the  $^{93}\text{Nb}$  NMR signal peaks are equal to  $h_{\text{loc}} = \nu_{\text{res}}/^{93}\gamma = 160.0$  kOe and  $h_{\text{loc}} = 158.1$  kOe for the compositions with  $x = 0.33$  and  $x = 0.5$ , correspondingly.

According to the calculation results the maximum value of the dipole field (similarly to the chromium nuclei in Sec. III A) induced on the niobium ion from the magnetic neighbors of chromium ions is observed for the crystal structures  $P6_322$   $h_{\text{loc,dip}} = -610$  Oe/ $\mu_B$ . That is why the  $\mathbf{h}_{\text{loc,hf}}$  hyperfine field for niobium ions as in the case of chromium ions is predominant.

Niobium ions in the  $\text{Cr}_x\text{NbSe}_2$  crystal structure have a trigonal-prismatic environment of six selenium atoms. Therefore, its 4d orbitals splitting has the same view as shown in Fig. 3. In the  $\text{NbSe}_2$  parent compound niobium is in the  $\text{Nb}^{4+}$  state, which implies that one 4d electron occupying  $e'_g$  orbitals remains in its valence shell. Intercalation of this compound with chromium leads to the addition of electrons to Nb-Se layers. One in  $\text{Cr}_{0.33}\text{NbSe}_2$  and one and a half electrons in the case  $\text{Cr}_{0.5}\text{NbSe}_2$  are added per  $\text{NbSe}_2$  formula unit. This means that the  $\text{Nb}^{4+}$  ion turns into  $\text{Nb}^{3+}$  with two electrons in the 4d shell in the first compound and turns into  $\text{Nb}^{2.5+}$  with 2.5 electrons in the 4d orbitals in the second case. Valence “2.5+” means that the same number of  $\text{Nb}^{3+}$  and  $\text{Nb}^{2+}$  ions in the system takes place, but since the 4d niobium electrons are

delocalized and mutual transformations of  $\text{Nb}^{3+} \leftrightarrow \text{Nb}^{2+}$  occur with a high rate,  $\nu_{\text{res}} = 1/\tau < 6 \times 10^9 \text{ s}^{-1}$ , these changes in the niobium electronic state are indistinguishable in the NMR experiment.

The local field in the location of the Nb nuclei at  $T < T_C$  could be the result of hybridization of chromium  $3d_{z^2}$  orbitals with niobium  $4d_{z^2}$  orbitals. In the literature, the hyperfine coupling constant for an electron on a  $4d$  orbit has a range of values:  $A = -210 \text{ kOe}/\mu_B$  [44],  $-310 \text{ kOe}/\mu_B$  [33], and  $-350 \text{ kOe}/\mu_B$  [29]. Therefore, we obtain, that for the creation of the field  $h_{\text{loc}} = 160.0 \text{ kOe}$ , the presence of a magnetic moment  $\mu \approx 0.46\text{--}0.76 \mu_B$  in the Nb  $4d$  shell is required, which is hardly possible with regard to the occupancy of the Cr  $3d_{z^2}$  orbital with  $n = 0.76$ . The  $h_{\text{loc}}$  induction on Nb nuclei due to the overlap of the unoccupied Nb  $5s$  orbital with the chromium  $3d_{z^2}$  orbital appears to be more probable. One electron in the Nb  $5s$  orbital creates a hyperfine field on the nucleus equal to  $2480 \text{ kOe}$  [44]. Therefore, to create the field  $h_{\text{loc}} = 160.0 \text{ kOe}$ , the polarization of only  $n = 0.06$  electrons in the  $5s$  shell is sufficient. If chromium  $3d_{z^2}$  electrons partially occupy niobium  $4d_{z^2}$  orbitals, then this value ( $n = 0.06$ ) should be larger, since the local magnetic fields induced on the nuclei by  $4d$  and  $5s$  electrons have a different sign. The slight difference in the local fields at the location of niobium nuclei in  $\text{Cr}_{0.5}\text{NbSe}_2$  ( $h_{\text{loc}} = 158.1 \text{ kOe}$  and  $\text{Cr}_{0.33}\text{NbSe}_2$  ( $h_{\text{loc}} = 160.0 \text{ kOe}$ ) apparently results from a difference in the values of the  $c$  lattice parameter of these compounds [6] and, therefore, in the degree of overlap of the electron shells of niobium and chromium ions. The local field on niobium nuclei is obviously induced by Cr ions, and not by the field from the ordered magnetic moments of the Nb intrinsic  $4d$  electrons. This is indirectly confirmed by the wider resonance line  $^{93}\text{Nb}$  and  $\text{Cr}_{0.33}\text{NbSe}_2$  compared to  $\text{Cr}_{0.5}\text{NbSe}_2$  (see Fig. 4). It was mentioned above that, in the composition of  $\text{Cr}_{0.33}\text{NbSe}_2$ , the regions with structures described by the  $P6_3/mmc$  and  $P6_322$  space groups can coexist. In this case, one can expect a greater disorder in the distribution of chromium near niobium ions and, therefore, a larger width of the NMR line. If the local fields on niobium nuclei were determined only by the intrinsic electrons of the Nb ions, then the width of the resonance lines of  $^{93}\text{Nb}$  in both compounds would hardly differ so noticeably.

The width of the NMR spectrum for  $^{93}\text{Nb}$  nuclei with a large quadrupole moment  $eQ$  and located in a noncubic environment is anomalously small. At first glance, the observed signal can also be attributed to the NMR response from the  $^{77}\text{Se}$  nuclei. For instance, in [45–47], the Cr valence state close to “4+” is explained as a result of a strong overlap between the Cr  $3d$  orbitals and Se  $4p$  orbitals. Spin polarization transfer between Cr and Se ions was observed in the selenide spinel compounds, where a large hyperfine field of  $80\text{--}100 \text{ kOe}$  was detected on the “nonmagnetic” Se ions by  $^{77}\text{Se}$  NMR spectroscopy. However, the presence of quadrupole beats (Fig. 5) in the spin-echo attenuation gives an answer to the following question: From which nucleus,  $^{77}\text{Se}$  or  $^{93}\text{Nb}$ , does the signal emanate? Obviously, this signal is not associated with selenium, since the  $^{77}\text{Se}$  nucleus with spin  $I = 1/2$  does not have a quadrupole moment [47,48], in contrast to  $^{93}\text{Nb}$ . In Fig. 5, the dependencies of spin-echo amplitude  $E(2t_{\text{del}})$  on the delay between pulses  $t_{\text{del}}$  in the sequence  $p\text{--}t_{\text{del}}\text{--}2p\text{--}t_{\text{del}}\text{--}E(2t_{\text{del}})$  are

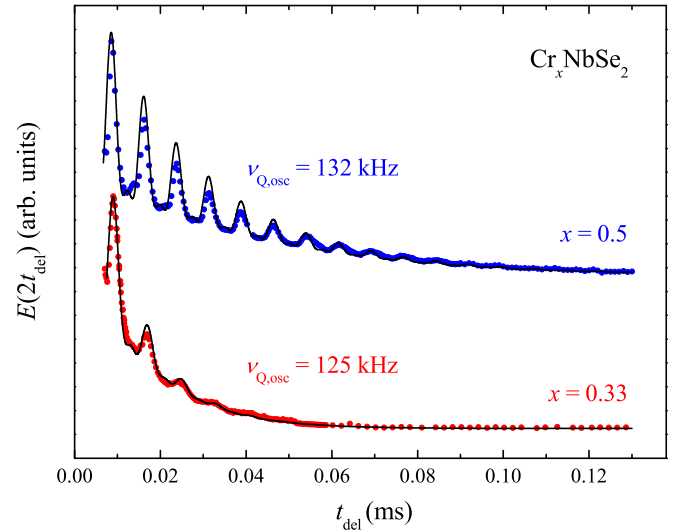


FIG. 5. Dependencies of spin-echo  $E(2t_{\text{del}})$  amplitude on the delay between pulses  $t_{\text{del}}$ , measured at maximum intensity of signals in the  $^{93}\text{Nb}$  NMR spectrum (Fig. 4) in  $\text{Cr}_x\text{NbSe}_2$  ( $x = 0.33, 0.5$ ). Solid lines show the result of extrapolation by function (4).

displayed for polycrystalline samples  $\text{Cr}_x\text{NbSe}_2$  ( $x = 0.33, 0.5$ ) at  $T = 4.2 \text{ K}$ . It is seen that  $E(2t_{\text{del}})$  is an exponentially decaying sinusoidal oscillation. It was shown in [49–52] that if the homogeneous magnetic broadening of the NMR line is less than the quadrupole line splitting, the oscillations appear in the spin-echo attenuation; the period of such oscillations is determined by the quadrupole frequency:

$$E(t) = B_1 \cos(2\pi \nu_{Q,\text{osc}} t) + B_2 \cos(4\pi \nu_{Q,\text{osc}} t) + \dots + B_N \cos(N\pi \nu_{Q,\text{osc}} t). \quad (4)$$

where  $B_1, B_2, B_3, B_4 \dots B_N$  are the oscillation amplitudes;  $\nu_{Q,\text{osc}}$  is the quadrupole frequency obtained from  $E(2t)$  modeling.

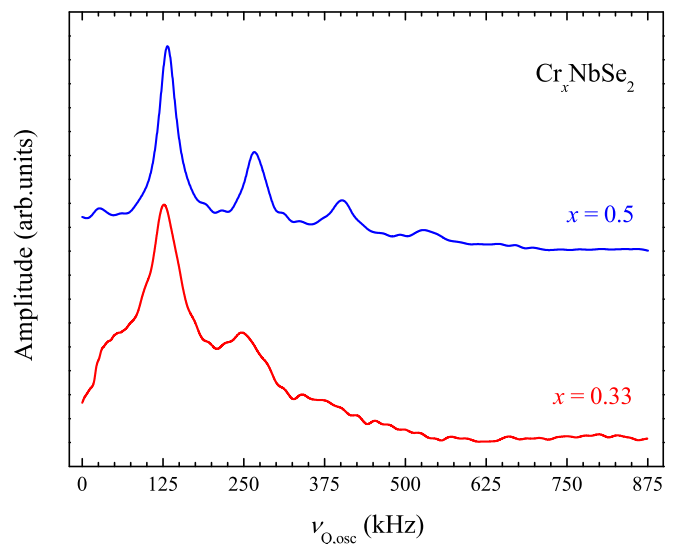


FIG. 6. Fourier transform of the signal  $E(2t_{\text{del}})$  on the  $^{93}\text{Nb}$  to  $\text{Cr}_x\text{NbSe}_2$  (Fig. 5).

The Fourier transform  $E(2t_{\text{del}})$  shown in Fig. 6 demonstrates the oscillation spectrum  $\nu_{\text{Q,osc}}$ . Several frequencies are observed in oscillations  $E(2t_{\text{del}})$ . The presence of such a high-order harmonic (for spin  $I = 9/2$  up to  $8\nu_{\text{Q,osc}}$ ) is discussed in detail in [50,51]. For example, the appearance of harmonics with the  $2\nu_{\text{Q,osc}}$  frequency in spin-echo attenuation for spin  $I = 9/2$  results from the simultaneous excitation of not only the nearest lines (for example,  $m_{-5/2 \leftrightarrow -3/2}$  and  $m_{-3/2 \leftrightarrow -1/2}$ ,  $m_{-3/2 \leftrightarrow -1/2}$ , and  $m_{-1/2 \leftrightarrow 1/2}$ , and so on), but also of the next line in the multiplet of the NMR spectrum (for example,  $m_{-5/2 \leftrightarrow -3/2}$  and  $m_{-1/2 \leftrightarrow 1/2}$ ,  $m_{-3/2 \leftrightarrow -1/2}$ , and  $m_{1/2 \leftrightarrow 3/2}$ ).

In our experiments, the effective excitation band at the duration of the second pulse  $2p = 2\mu\text{s}$  was  $\Delta\nu \approx 1/p \approx 500\text{ kHz}$ . Therefore, it may be expected that at a spectrum width of  $\Delta\nu \approx 6\text{ MHz}$ , not only harmonics with one  $\nu_{\text{Q,osc}}$  frequency are excited effectively, but also harmonics of the higher order. For the  $\text{Cr}_{0.5}\text{NbSe}_2$  sample, the Fourier transform  $E(2t_{\text{del}})$  demonstrates the spectrum of emerging oscillations up to  $4\nu_{\text{Q,osc}} \approx 528\text{ kHz}$ , which is in good agreement with the effective excitation band  $\Delta\nu \approx 500\text{ kHz}$ .

The  $E(2t_{\text{del}})$  data given in Fig. 5 are well extrapolated by the function

$$\begin{aligned} E(2t_{\text{del}}) \propto & \exp(-t/T_2) + \exp(-t/T_2^*) \\ & \times [1 + B_1 \cos(\pi \nu_{\text{Q,osc}} t_{\text{del}}) \\ & + B_2 \cos(2\pi \nu_{\text{Q,osc}} t_{\text{del}}) + B_3 \cos(3\pi \nu_{\text{Q,osc}} t_{\text{del}}) \\ & + B_4 \cos(4\pi \nu_{\text{Q,osc}} t_{\text{del}})] \end{aligned} \quad (5)$$

at the following parameter values:  $B_{1,2,3,4} < 1$  is oscillation amplitude,  $T_2 = 13\mu\text{s}$ ,  $T_2^* = 7\mu\text{s}$ ,  $\nu_{\text{Q,osc}} = 125(35)\text{ kHz}$  for  $\text{Cr}_{0.33}\text{NbSe}_2$ ;  $T_2 = 32\mu\text{s}$ ,  $T_2^* = 19\mu\text{s}$ ,  $\nu_{\text{Q,osc}} = 132(14)\text{ kHz}$  for  $\text{Cr}_{0.5}\text{NbSe}_2$ ;  $1/T_2$  is spin-spin relaxation rate;  $1/T_2^*$  is the oscillations attenuation rate.

The calculations of quadrupole interaction parameters of the niobium nucleus in the crystal structures  $P6_3/mmc$  and  $P6_322$  were performed using the first-principles calculations. In both crystal structures, the main axis of the electric-field gradient  $V_{zz}$  on niobium nuclei was directed along the  $c$  axis with asymmetry parameter  $\eta$  close to zero. The quadrupole frequency for the crystal structures  $P6_322$  was  $\nu_{\text{Q}}^{\text{calc}} \approx 1.2\text{ MHz}$ . In the crystal structures  $P6_3/mmc$ , the distribution of frequencies was from 1.2 to 0.8 MHz. Such a  $\nu_{\text{Q}}^{\text{calc}}$  distribution is associated with the existence of nonequivalent niobium positions in the structure due to the different nearest environment of chromium ions. Taking into account that the chromium magnetic moments are arranged in the  $ab$  plane and the principal EFG axis  $V_{zz}$  is directed along the  $c$  axis, the frequency obtained from the beats of spin-spin relaxation is one half of  $\nu_{\text{Q}} = 2\nu_{\text{Q,osc}} = 264(2)\text{ kHz}$ . Thus the distance between the most distant satellites of the  $^{93}\text{Nb}$  NMR quadrupole spectrum (between the satellites corresponding to the  $+9/2 \leftrightarrow +7/2$  and  $-9/2 \leftrightarrow -7/2$  transitions) is about 1 MHz. Such a distance is less than the experimentally observed width of the  $^{93}\text{Nb}$  NMR lines (full width at half maximum  $\Delta \approx 2\text{ MHz}$  for  $\text{Cr}_{0.5}\text{NbSe}_2$  and  $\Delta \approx 4\text{ MHz}$  for  $\text{Cr}_{0.33}\text{NbSe}_2$ ) shown in Fig. 4; the broadening of these lines is suggestive of being magnetic rather than quadrupole in nature. The ex-

perimental and calculated values of the quadrupole frequency differ by more than four times. This can be attributed to the inhomogeneous distribution of chromium ions over the lattice, which significantly complicates the indication of the crystal lattice for calculations. It is worth mentioning that when searching for the  $^{93}\text{Nb}$  response in our  $\text{Cr}_x\text{NbSe}_2$  samples, the NMR signal was detected in a wide frequency range:  $\nu = 100\text{--}176\text{ MHz}$  (Fig. 4); however, the signal intensity in the frequency range  $100\text{--}150\text{ MHz}$  turned out to be at least 50 times lower than the intensity at frequencies around 166 MHz (see inset in Fig. 4). Unfortunately, we do not have an unambiguous answer about the nature of the low-intensity NMR lines observed in this frequency range. It is possible that these lines are associated with the presence of a small amount of foreign phases in the samples.

#### IV. CONCLUSION

Using the methods of NMR on  $^{53}\text{Cr}$  and  $^{93}\text{Nb}$  nuclei, polycrystalline samples of magnetically ordered chalcogenides  $\text{Cr}_x\text{NbSe}_2$  ( $x = 0.33, 0.5$ ) were investigated in zero external magnetic field at temperature  $T = 4.2\text{ K}$ . The first-principles calculation of the parameters of the quadrupole interaction of chromium and niobium nuclei in compounds  $\text{Cr}_x\text{NbSe}_2$  ( $x = 0.33, 0.5$ ) for the structures described by space groups  $P6_3/mmc$  and  $P6_322$  was performed in order to analyze the NMR data. A comprehensive analysis of NMR data and calculations allowed us to suggest the crystal structure of the  $\text{Cr}_{0.5}\text{NbSe}_2$  compound can rather be characterized as belonging to the space group  $P6_322$ . It has been obtained that, for both structures, the principal axis of the electric-field gradient  $V_{zz}$  on the positions of Nb and Cr nuclei is directed along the  $c$  axis and the asymmetry parameter is close to zero. An estimation of the dipole field in the magnetically ordered state has shown that its contribution to the local magnetic field which defines the frequency of NMR chromium  $^{53}\nu_{\text{res}}$  nuclei and niobium  $^{93}\nu_{\text{res}}$  nuclei is not significant in comparison with the hyperfine field, and the dipole field can be neglected. Using the analysis of the hyperfine field on  $^{53}\text{Cr}$  nuclei, the average value of the chromium magnetic moment was determined as  $\mu_{\text{NMR}} \approx 2.2\mu_{\text{B}}$  which is lower than the theoretical value  $3\mu_{\text{B}}$  for  $\text{Cr}^{3+}$  and closer to  $2\mu_{\text{B}}$  for  $\text{Cr}^{4+}$ . The presence of the local magnetic field  $h_{\text{loc}} \approx 160\text{ kOe}$  on Nb nuclei is shown experimentally. These observations are explained by the high degree of hybridization of  $a_{1g}$  and  $e_g$  orbitals of  $3d$  Cr electrons with  $4d_{z^2}$  and  $5s$  niobium orbitals. It should be noted that lower values of the magnetic moment of the intercalated atoms in comparison with the theoretical spin value were obtained using neutron diffraction for other intercalated compounds exhibiting a long-range magnetic order (see [53–55], for example); the reduction of a magnetic moment of  $M'$  atoms in  $M'_xMX_2$  was ascribed to the hybridization effects of  $3d$  electrons of intercalated atoms with electronic states of the  $MX_2$  host lattice. Moreover, in  $\text{Fe}_x\text{TiSe}_2$  the presence of a small induced magnetic moment on the Ti atoms was proposed to describe the antiferromagnetic structure of these compounds [54,56].

The results obtained in the present work demonstrate that NMR spectroscopy on various nuclei can provide useful

information for a deeper understanding of how the  $3d$  metal atoms with a magnetic moment being inserted into  $MX_2$  affect the distribution of electron and spin density in the intercalated compounds. These data, as well as the results obtained by other experimental methods and by means of calculations, show that changes in the electronic structure of TMDs as a result of intercalation can be significant and should be taken into account in developing new materials and applications.

## ACKNOWLEDGMENTS

The research was carried out within the state assignment of Ministry of Science and Higher Education of the Russian Federation (Theme “Function” No. AAAA-A19-119012990095-0). N.M.N. thanks the Competitiveness Enhancement Program of the Ural Federal University No. CEP 3.1.1.1-20 for financial support.

- 
- [1] A. B. Kaul, Two-dimensional layered materials: Structure, properties, and prospects for device applications, *J. Mater. Res.* **29**, 348 (2014).
- [2] J. A. Wilson and A. D. Yoffe, The transition metal dichalcogenides discussion and interpretation of the observed optical, electrical and structural properties, *Adv. Phys.* **18**, 193 (1969).
- [3] I. Guillamón, H. Suderow, S. Vieira, L. Cario, P. Diener, and P. Rodiere, Superconducting Density of States and Vortex Cores of  $2H$ -NbS<sub>2</sub>, *Phys. Rev. Lett.* **101**, 166407 (2008).
- [4] S. S. P. Parkin and R. H. Friend,  $3d$  transition-metal intercalates of the niobium and tantalum dichalcogenides. I. Magnetic properties, *Philos. Mag. B* **41**, 65 (1980).
- [5] Y. Cao, Z. Huang, Y. Yin, H. Xie, B. Liu, W. Wang, C. Zhu, D. Mandrus, L. Wang, and W. Huang, Overview and advances in a layered chiral helimagnet Cr<sub>1/3</sub>NbS<sub>2</sub>, *Mater. Today Adv.* **7**, 100080 (2020).
- [6] N. M. Toporova, E. M. Sherokalova, N. V. Selezneva, V. V. Ogloblichev, and N. V. Baranov, Crystal structure, properties and Griffiths-like phase in niobium diselenide intercalated with chromium, *J. Alloys Compd.* **848**, 156534 (2020).
- [7] T. Moriya and T. Miyadai, Evidence for the helical spin structure due to antisymmetric exchange interaction in Cr<sub>1/3</sub>NbS<sub>2</sub>, *Solid State Commun.* **42**, 209 (1982).
- [8] Y. Togawa, T. Koyama, K. Takayanagi, S. Mori, Y. Kousaka, J. Akimitsu, S. Nishihara, K. Inoue, A. S. Ovchinnikov, and J. Kishine, Chiral Magnetic Soliton Lattice on a Chiral Helimagnet, *Phys. Rev. Lett.* **108**, 107202 (2012).
- [9] N. J. Ghimire, M. A. McGuire, D. S. Parker, B. Sipos, S. Tang, J.-Q. Yan, and D. Mandrus, Magnetic phase transition in single crystals of the chiral helimagnet Cr<sub>1/3</sub>NbS<sub>2</sub>, *Phys. Rev. B* **87**, 104403 (2013).
- [10] K. Tsuruta, M. Mito, H. Deguchi, J. Kishine, Y. Kousaka, J. Akimitsu, and K. Inoue, Phase diagram of the chiral magnet Cr<sub>1/3</sub>NbS<sub>2</sub> in a magnetic field, *Phys. Rev. B* **93**, 104402 (2016).
- [11] Y. Togawa, T. Koyama, Y. Nishimori, Y. Matsumoto, S. McVitie, D. McGrouther, R. L. Stamps, Y. Kousaka, J. Akimitsu, S. Nishihara, K. Inoue, I. G. Bostrem, V. E. Sinitsyn, A. S. Ovchinnikov, and J. Kishine, Magnetic soliton confinement and discretization effects arising from macroscopic coherence in a chiral spin soliton lattice, *Phys. Rev. B* **92**, 220412(R) (2015).
- [12] L. Wang, N. Chepiga, D.-K. Ki, L. Li, F. Li, W. Zhu, Y. Kato, O. S. Ovchinnikova, F. Mila, I. Martin, D. Mandrus, and A. F. Morpurgo, Controlling the Topological Sector of Magnetic Solitons in Exfoliated Cr<sub>1/3</sub>NbS<sub>2</sub> Crystals, *Phys. Rev. Lett.* **118**, 257203 (2017).
- [13] A. F. Gubkin, E. P. Proskurina, Y. Kousaka, E. M. Sherokalova, N. V. Selezneva, J. P. Miao, S. Lee, J. Zhang, Y. Ishikawa, S. Torii, T. Kamiyama, J. Campo, J. Akimitsu, and N. V. Baranov, Crystal and magnetic structures of Cr<sub>1/3</sub>NbSe<sub>2</sub> from neutron diffraction, *J. Appl. Phys.* **119**, 013903 (2016).
- [14] N. Sirica, S.-K. Mo, F. Bondino, I. Pis, S. Nappini, P. Vilmercati, J. Yi, Z. Gai, P. C. Snijders, P. K. Das, I. Vobornik, N. Ghimire, M. R. Koehler, L. Li, D. Sapkota, D. S. Parker, D. G. Mandrus, and N. Mannella, Electronic structure of the chiral helimagnet and  $3d$ -intercalated transition metal dichalcogenide Cr<sub>1/3</sub>NbS<sub>2</sub>, *Phys. Rev. B* **94**, 075141 (2016).
- [15] N. Sirica, P. Vilmercati, F. Bondino, I. Pis, S. Nappini, S.-K. Mo, A. V. Fedorov, P. K. Das, I. Vobornik, J. Fujii, L. Li, D. Sapkota, D. S. Parker, D. G. Mandrus, and N. Mannella, The nature of ferromagnetism in the chiral helimagnet Cr<sub>1/3</sub>NbS<sub>2</sub>, *Commun. Phys.* **3**, 1 (2020).
- [16] W. Z. Hu, G. T. Wang, R. Hu, C. Petrovic, E. Morosan, R. J. Cava, Z. Fang, and N. L. Wang, Evidence for a band broadening across the ferromagnetic transition of Cr<sub>1/3</sub>NbSe<sub>2</sub>, *Phys. Rev. B* **78**, 085120 (2008).
- [17] S. Kobayashi, N. Katayama, T. Manjo, H. Ueda, C. Michioka, J. Sugiyama, Y. Sassa, O. K. Forslund, M. Månsson, K. Yoshimura, and H. Sawa, Linear trimer formation with antiferromagnetic ordering in  $1T$ -CrSe<sub>2</sub> originating from Peierls-like instabilities and interlayer Se–Se interactions, *Inorg. Chem.* **58**, 14304 (2019).
- [18] A. F. Sadykov, A. P. Gerashchenko, Yu. V. Piskunov, V. V. Ogloblichev, A. G. Smol’nikov, S. V. Verkhovskii, A. Yu. Yakubovskii, E. A. Tishchenko, and A. A. Bush, Magnetic structure of low-dimensional LiCu<sub>2</sub>O<sub>2</sub> multiferroic according to <sup>63,65</sup>Cu and <sup>7</sup>Li NMR studies, *J. Exp. Theor. Phys.* **115**, 666 (2012).
- [19] V. V. Ogloblichev, Yu. V. Piskunov, and F. B. Mushenok, Magnetic order in the structurally disordered helicoidal magnet Cr<sub>1/3</sub>NbS<sub>2</sub>: NMR at <sup>53</sup>Cr nuclei, *J. Exp. Theor. Phys.* **125**, 317 (2017).
- [20] A. F. Sadykov, A. P. Gerashchenko, Yu. V. Piskunov, V. V. Ogloblichev, A. G. Smol’nikov, S. V. Verkhovskii, A. L. Buzlukov, I. Yu. Arapova, Y. Furukawa, A. Yu. Yakubovskii, and A. A. Bush, Magnetic structure of the low-dimensional magnet NaCu<sub>2</sub>O<sub>2</sub>: <sup>63,65</sup>Cu and <sup>23</sup>Na NMR studies, *J. Exp. Theor. Phys.* **119**, 870 (2014).
- [21] A. G. Smol’nikov, V. V. Ogloblichev, S. V. Verkhovskii, K. N. Mikhalev, A. Yu. Yakubovskii, Y. Furukawa, Yu. V. Piskunov, A. F. Sadykov, S. N. Barilo, and S. V. Shiryayev, Specific features of magnetic order in a multiferroic compound CuCrO<sub>2</sub> determined using NMR and NQR data for <sup>63,65</sup>Cu nuclei, *Phys. Met. Metallogr.* **118**, 134 (2017).

- [22] G. Kresse and D. Joubert, From ultrasoft pseudopotentials to the projector augmented-wave method, *Phys. Rev. B* **59**, 1758 (1999).
- [23] J. P. Perdew, K. Burke, and M. Ernzerhof, Generalized Gradient Approximation Made Simple, *Phys. Rev. Lett.* **77**, 3865 (1996); Generalized Gradient Approximation Made Simple [Phys. Rev. Lett. **77**, 3865 (1996)], **78**, 1396(E) (1997).
- [24] G. Kresse and J. Furthmüller, Efficiency of *ab-initio* total energy calculations for metals and semiconductors using a plane-wave basis set, *Comput. Mater. Sci.* **6**, 15 (1996).
- [25] C. P. Slichter, *Principles of Magnetic Resonance* (Harper & Row, New York, 1963).
- [26] K. Ishida, Y. Niino, G.-Q. Zheng, Y. Kitaoka, K. Asayama, and T. Ohtani,  $^{93}\text{Nb}$  NQR study in layered superconducting  $2\text{H-NbSe}_2$ , *J. Phys. Soc. Jpn.* **65**, 2341 (1996).
- [27] V. Dyadkin, F. Mushenok, A. Bosak, D. Menzel, S. Grigoriev, P. Pattison, and D. Chernyshov, Structural disorder versus chiral magnetism in  $\text{Cr}_{1/3}\text{NbS}_2$ , *Phys. Rev. B* **91**, 184205 (2015).
- [28] Z. Dai, Q. Xue, Y. Gong, C. G. Slough, and R. V. Coleman, Scanning-probe-microscopy studies of superlattice structures and density-wave structures in  $2\text{H-NbSe}_2$ ,  $2\text{H-TaSe}_2$ , and  $2\text{H-TaS}_2$  induced by Fe doping, *Phys. Rev. B* **48**, 14543 (1993).
- [29] A. Freeman and R. Frankel, *Hyperfine Interactions* (Academic Press, New York, 1967).
- [30] L. D. Landau and E. M. Lifshitz, *The Classical Theory of Fields: Vol. 2*, 4th ed., Course of Theoretical Physics Series (Butterworth-Heinemann, Oxford, 1975).
- [31] V. V. Ogloblichev, A. F. Sadykov, Y. Furukawa, Q. P. Ding, A. G. Smolnikov, Y. V. Piskunov, K. N. Mikhalev, A. P. Gerashenko, A. Wu, S. N. Barilo, and S. V. Shiryayev,  $^{63,65}\text{Cu}$  NMR study of the magnetically ordered state of the multiferroic  $\text{CuFeO}_2$ , *J. Magn. Magn. Mater.* **504**, 166668 (2020).
- [32] M. Mito, H. Ohsumi, T. Shishidou, F. Kuroda, M. Weinert, K. Tsuruta, Y. Kotani, T. Nakamura, Y. Togawa, J. Kishine, Y. Kousaka, J. Akimitsu, and K. Inoue, Observation of orbital angular momentum in the chiral magnet  $\text{CrNb}_3\text{S}_6$  by soft x-ray magnetic circular dichroism, *Phys. Rev. B* **99**, 174439 (2019).
- [33] A. K. Koh and D. J. Miller, Hyperfine coupling constants and atomic parameters for electron paramagnetic resonance data, *At. Data Nucl. Data Tables* **33**, 235 (1985).
- [34] M. Rubinstein, G. Stauss, and J. Krebs, Nuclear magnetic resonance of  $\text{Cr}^{53}$  in antiferromagnetic  $\text{Cr}_2\text{O}_3$ , *Phys. Lett.* **12**, 302 (1964).
- [35] V. G. Pleschov, N. V. Baranov, A. N. Titov, K. Inoue, M. I. Bartashevich, and T. Goto, Magnetic properties of Cr-intercalated  $\text{TiSe}_2$ , *J. Alloys Compd.* **320**, 13 (2001).
- [36] N. V. Selezneva, E. M. Sherokalova, V. G. Pleshchev, V. A. Kazantsev, and N. V. Baranov, Suppression and inducement of the charge-density-wave state in  $\text{Cr}_x\text{TiSe}_2$ , *J. Phys.: Condens. Matter* **28**, 315401 (2016).
- [37] A. S. Shkvarin, Y. M. Yarmoshenko, A. I. Merentsov, I. Pis, F. Bondino, E. G. Shkvarina, and A. N. Titov, Guest-host chemical bonding and possibility of ordering of intercalated metals in transition-metal dichalcogenides, *Inorg. Chem.* **57**, 5544 (2018).
- [38] E. G. Shkvarina, S. G. Titova, A. N. Titov, and A. S. Shkvarin, The mechanism of the formation of one-dimensional chains of the iron and vanadium atoms in the  $\text{TiSe}_2$  interlayer space, *J. Alloys Compd.* **717**, 286 (2017).
- [39] A. S. Shkvarin, M. V. Yablonkikh, Yu. M. Yarmoshenko, A. I. Merentsov, B. V. Senkovskiy, J. Avila, M. Asensio, and A. N. Titov, Electronic structure of octahedrally coordinated Cr in  $\text{Cr}_x\text{TiX}_2$  ( $X = \text{Se}, \text{Te}$ ) and  $\text{Ti}_x\text{Cr}_{1-x}\text{Se}$ , *J. Electron Spectrosc. Relat. Phenom.* **206**, 12 (2016).
- [40] Z. H. Han, J. I. Budnick, W. A. Hines, B. Dabrowski, S. Kolesnik, and T. Maxwell, Nuclear magnetic resonance study of the enhanced ferromagnetic ordering in polycrystalline  $\text{SrRu}_{1-x}\text{Cr}_x\text{O}_3$  ( $0 \leq x \leq 0.12$ ), *J. Phys.: Condens. Matter* **17**, 1193 (2005).
- [41] H. Takeda, Y. Shimizu, Y. Kobayashi, M. Itoh, T. Jin-no, M. Isobe, Y. Ueda, S. Yoshida, Y. Muraoka, and T. Yokoya, Local electronic state in the half-metallic ferromagnet  $\text{CrO}_2$  investigated by site-selective  $^{53}\text{Cr}$  NMR measurements, *Phys. Rev. B* **93**, 235129 (2016).
- [42] D. M. Bishop, *Group Theory and Chemistry* (Dover, New York, 1993).
- [43] O. B. Lapina, D. F. Khabibulin, K. V. Romanenko, Z. Gan, M. G. Zuev, V. N. Krasil'nikov, and V. E. Fedorov,  $^{93}\text{Nb}$  NMR chemical shift scale for niobia systems, *Solid State Nucl. Magn. Reson.* **28**, 204 (2005).
- [44] V. Yafet and V. Jaccarino, Nuclear spin relaxation in transition metals; core polarization, *Phys. Rev.* **133**, A1630 (1964).
- [45] S. Park, S. Kwon, S. Lee, S. Khim, D. Bhoi, C. B. Park, and K. H. Kim, Interactions in the bond-frustrated helimagnet  $\text{ZnCr}_2\text{Se}_4$  investigated by NMR, *Sci. Rep.* **9**, 16627 (2019).
- [46] S. Berger, J. Budnick, and T. Burch, NMR of  $^{53}\text{Cr}$  and  $^{77}\text{Se}$  in ferromagnetic chalcogenide spinels, *J. Appl. Phys.* **39**, 658 (1968).
- [47] S. Kobayashi, H. Ueda, D. Nishio-Hamane, C. Michioka, and K. Yoshimura, Successive phase transitions driven by orbital ordering and electron transfer in quasi-two-dimensional  $\text{CrSe}_2$  with a triangular lattice, *Phys. Rev. B* **89**, 054413 (2014).
- [48] B. A. Demko and R. E. Wasylshen, Solid-state selenium-77 NMR, *Prog. Nucl. Magn. Reson. Spectrosc.* **54**, 208 (2009).
- [49] V. V. Ogloblichev, A. G. Smolnikov, A. F. Sadykov, Y. V. Piskunov, A. P. Gerashenko, Y. Furukawa, K. Kumagai, A. Y. Yakubovsky, K. N. Mikhalev, S. N. Barilo, S. V. Shiryayev, and A. S. Belozero,  $^{17}\text{O}$  NMR study of the triangular lattice antiferromagnet  $\text{CuCrO}_2$ , *J. Magn. Magn. Mater.* **458**, 1 (2018).
- [50] H. Alloul and C. Froidevaux, Nuclear-magnetic-resonance spin echoes in alloys, *Phys. Rev.* **163**, 324 (1967).
- [51] H. Abe, H. Yasuoka, and A. Hirai, Spin echo modulation caused by the quadrupole interaction and multiple spin echoes, *J. Phys. Soc. Jpn.* **21**, 77 (1966).
- [52] A. G. Smol'nikov, V. V. Ogloblichev, A. F. Sadykov, Yu. V. Piskunov, A. P. Gerashchenko, S. V. Verkhovskii, A. Yu. Yakubovskii, S. N. Barilo, G. L. Bychkov, and S. V. Shiryayev, NMR study of the electric field gradient in the paramagnetic phase of  $M_3\text{V}_2\text{O}_8$  ( $M = \text{Co}, \text{Ni}$ ) compounds, *J. Exp. Theor. Phys.* **112**, 1020 (2011).
- [53] P. Vaqueiro, M. L. Kosidowski, and A. V. Powell, Structural distortions of the metal dichalcogenide units in  $\text{AMo}_2\text{S}_4$  ( $A = \text{V}, \text{Cr}, \text{Fe}, \text{Co}$ ) and magnetic and electrical properties, *Chem. Mater.* **14**, 1201 (2002).

- [54] N. V. Selezneva, N. V. Baranov, V. G. Pleshchev, N. V. Mushnikov, and V. I. Maksimov, Magnetic state and properties of the  $\text{Fe}_{0.5}\text{TiSe}_2$  intercalation compound, *Phys. Solid State* **53**, 329 (2011).
- [55] N. V. Baranov, E. M. Sherokalova, N. V. Selezneva, A. V. Proshkin, L. Keller, A. S. Volegov, and E. P. Proskurina, Magnetic order, field induced phase transition and magnetoresistance in the intercalated compound  $\text{Fe}_{0.5}\text{TiS}_2$ , *J. Phys.: Condens. Matter* **25**, 066004 (2013).
- [56] G. Calvarin, J. R. Gavarrı, M. A. Buhannic, P. Colombet, and M. Danot, Crystal and magnetic structures of  $\text{Fe}_{0.25}\text{TiSe}_2$  and  $\text{Fe}_{0.48}\text{TiSe}_2$ , *Rev. Phys. Appl.* **22**, 1131 (1987).